








Elucidation of CKAP4-remodeled cell mechanics in driving metastasis of bladder cancer through aptamer-based target discovery

Xing Sun^{a,1}, Lin Xie^{a,1}, Siyuan Qiu^{a,1} , Hui Li^{a,1} , Yangyang Zhou^a , Hui Zhang^{a,b}, Yibin Zhang^a, Lin Zhang^a, Tiantian Xie^a, Yinglei Chen^a, Lili Zhang^a, Zilong Zhao^a , Tianhuan Peng^a, Jing Liu^{c,d}, Wencan Wu^e, Lei Zhang^f, Juan Li^b , Mao Ye^{a,2}, and Weihong Tan^{a,b,2}

Edited by Jay Groves, University of California, Berkeley, CA; received June 7, 2021; accepted February 21, 2022 by Editorial Board Member Chad A. Mirkin

Metastasis contributes to the dismal prognosis of bladder cancer (BLCA). The mechanical status of the cell membrane is expected to mirror the ability of cell migration to promote cancer metastasis. However, the mechanical characteristics and underlying molecular profile associated with BLCA metastasis remain obscure. To study the unique cellular architecture and traits associated with cell migration, using a process called cell-based systematic evolution of ligands by exponential enrichment (cell-SELEX) we generated an aptamer-based molecular probe, termed spl3c, which identified cytoskeleton-associated protein 4 (CKAP4). CKAP4 was associated with tumor metastasis in BLCA, but we also found it to be a mechanical regulator of BLCA cells through the maintenance of a central-to-peripheral gradient of stiffness on the cell membrane. Notably, such mechanical traits were transportable through exosome-mediated intercellular CKAP4 trafficking, leading to significant enhancement of migration in recipient cells and, consequently, aggravating metastatic potential *in vivo*. Taken together, our study shows the robustness of this aptamer-based molecular tool for biomarker discovery, revealing the dominance of a CKAP4-induced central-to-peripheral gradient of membrane stiffness that benefits cell migration and delineating the role of exosomes in mediating mechanical signaling in BLCA metastasis.

aptamer | bladder cancer | CKAP4 | cell mechanics | cell migration

Metastasis generally contributes to a dismal prognosis in BLCA cases. Elucidating how cells evolve into a metastatic phenotype, e.g., enhanced cell migration, leads to a better understanding of physical and pathological processes (1, 2). Architectural and mechanical traits, such as geometry, roughness, spreading, viscosity, and stiffness, are known to significantly affect migration ability (3–5). Since such features delineate how cancer cells perceive, deform, and adapt to the surrounding tumor microenvironment during progression, they have received extensive investigative attention (6–8).

Cell stiffness, which is gaining attention as a critical physical index of cellular adhesion to the extracellular matrix, the status of the cell cortex underneath the cell membrane, and characteristics of cell cytoskeleton organization, has been reported as an element that positively correlates with cell migration (8–10). Paradoxically, in some advanced cancer cells the stiffness has been reported to be lower than that of healthy cells (11–13). Studies have shown that stiffening benefits the mechanotransduction observed in cell migration and provides the necessary mechanical strength for cells to break through the rigid surrounding barriers, while cell softness allows for the deformation required for cells to work their way through narrow extracellular gaps during cancer metastasis (14–17). Thus far, no clear consensus has determined whether optimized stiffness or well-organized integration of diverse localized stiffness is more beneficial to cancer cell migration (8, 17–19). Notably, the formation of nano- or meso-scale domains on the cell membrane by clustered proteins/lipids and the dynamic organization of membrane-proximal F-actin gradient in the cytoplasm offer some clues regarding the coexistence of diverse surface mechanical traits involved in cell movement (20–23). Thus, understanding cancer metastasis depends in large part on knowledge about cell surface mechanotransduction and associated mechanical traits, such as stiffness, that contribute to cell migration.

Focal adhesion kinase (FAK) and transcription factors YAP/TAZ, as well as their signaling axis, are two key pathways that regulate the response of cells to mechanical changes in the extracellular matrix (11, 24, 25). The discovery of molecular profiles in the regulation of cell mechanics will offer a better understanding of how cells interact with their surrounding biological environment (19, 26). In this context, aptamers, which can specifically bind to their target by forming certain 3-dimensional structures, can act as a superior molecular tool to investigate the molecular profile of cells (27, 28).

Significance

Metastasis generally leads to a dismal prognosis in bladder cancer (BLCA). The mechanical status of the cell membrane has been reported to reflect the potential of the metastatic capacity of cancer cells. However, the molecular profile and corresponding mechanical traits underlying BLCA metastasis remain largely elusive. Our study demonstrates the significance of cytoskeleton-associated protein 4 (CKAP4) in BLCA malignancy through aptamer selection, emphasizes the mechanical dominance of the central-to-peripheral gradient over simply softening or stiffening in cell migration, and shows the role of exosomes in mediating mechanical signaling in BLCA metastasis. Altogether, our work verifies the promising advantages of an aptamer-based approach in cancer research, which ranges from biomarker discovery to the elucidation of biological functions.

The authors declare no competing interest.

This article is a PNAS Direct Submission. J.G. is a guest editor invited by the Editorial Board.

Copyright © 2022 the Author(s). Published by PNAS. This article is distributed under [Creative Commons Attribution-NonCommercial-NoDerivatives License 4.0 \(CC BY-NC-ND\)](https://creativecommons.org/licenses/by-nc-nd/4.0/).

¹X.S., L.X., S.Q., and H.L. contributed equally to this work.

²To whom correspondence may be addressed. Email: goldleaf@hnu.edu.cn or tan@hnu.edu.cn.

This article contains supporting information online at <http://www.pnas.org/lookup/suppl/doi:10.1073/pnas.2110500119/-DCSupplemental>.

Published April 11, 2022.

Accordingly, in this work, we develop an aptamer-based molecular tool, spl3c, and prove its robustness in biomarker discovery. We also report cytoskeleton-associated protein 4 (CKAP4) as a regulator of the mechanotransduction process, promoting the migration of BLCA cells through the maintenance of a central-to-peripheral gradient of stiffness on the cell membrane. We further show that mechanical traits can be intercellularly transported by CKAP4-bearing exosomes, leading to a significant enhancement of migration ability in recipient cells and aggravating cancer metastasis *in vivo*. Collectively, our work provides insights into how cells organize mechanical cues to drive cell migration and, finally cancer metastasis.

Results

Acquisition of an Aptamer-Based Molecular Tool Targeting BLCA Cells. To obtain a robust tool to uncover the characteristic molecular profile of BLCA cells, the cell-SELEX (cell systematic evolution of ligands by exponential enrichment) technique was used to screen for high-affinity aptamers against BLCA 5637 cells and normal human uroepithelial SV-HUC-1 cells. As the screening cycle proceeded, evident stepwise fluorescence accumulation was observed in the BLCA 5637 cells and reached maximum in the 13th cycle, indicating the enrichment of potential aptamer candidates in the screening DNA pool (Fig. 1*A*). Hierarchy cluster analysis for the top 20 dominant sequences, which constitute the majority of DNA sequences, in the DNA pool of the 13th cycle showed four clustered subgroups from which eight representative DNA sequences (spl1–spl8) were selected as aptamer candidates for further confirmation (Fig. 1*B* and *SI Appendix*, Fig. S1 and S2). Binding ability and specificity to the BLCA 5637 cells were evaluated by flow cytometry and cell imaging, and spl3 showed the best binding ability and specificity (Fig. 1*C* and *D*). Furthermore, in a broader spectrum of cell lines, spl3 showed the best binding to the BLCA 5637 and T24 cells, reduced binding to other adherent cancer cells, and almost no binding to normal human uroepithelial SV-HUC-1 and leukemia cells (Fig. 1*E*). In addition, according to the secondary structure and Gibbs free energy analysis, spl3 retained both excellent structural diversity and thermodynamic stability, suggesting its potential to be an outstanding aptamer-based molecular-level tool for BLCA investigation (*SI Appendix*, Fig. S2).

To optimize the aptamer sequence, aptamer truncation was performed (Fig. 1*F*). Among all five daughter sequences, spl3c showed the best binding ability (Fig. 1*G* and *SI Appendix*, Fig. S3), and truncation enhanced the binding affinity from 37.2 nM (spl3) to 21.3 nM (spl3c) (Fig. 1*H*), which may have resulted from the removal of superfluous nonfunctional nucleotides. The binding ability of spl3c to various cell lines was at a similar level as that of spl3 (*SI Appendix*, Fig. S4). Importantly, the binding sites of spl3c on the cells were almost the same as those of spl3, as demonstrated by competition assay (Fig. 1*I*). Both *in vivo* and *ex vivo* imaging showed that spl3c accumulated strongly in tumor sites, exhibited good biocompatibility and excellent stability, and could be internalized into cytosol, demonstrating its promising potential for tumor targeting and drug delivery (Fig. 1*J* and *K* and *SI Appendix*, Fig. S5 and S6).

Identification of the Target of spl3c in BLCA Cells. The target of aptamer spl3c was determined amid the complex composition of the cell membrane. Proteinase K and trypsin were used to deplete the proteins on the cell membrane before aptamer binding. As shown in Fig. 2*A*, both proteinase K and trypsin

treatment significantly mitigated the binding capacity of spl3c to the BLCA 5637 cells, suggesting that the target of spl3c might be a protein on the cell membrane. Then, aptamer-conjugated beads were used to capture the interacting proteins. As shown in Fig. 2*B*, two differential bands at 60 and 120 kDa were observed. Out of all purified proteins, mass spectroscopy (MS) showed that CKAP4 exhibited both a high score and marked fold change (Fig. 2*C* and *SI Appendix*, Fig. S7). Aptamer pull-down assay further indicated that the target of aptamer spl3c was CKAP4 (Fig. 2*D*). Meanwhile, by down- and up-regulation of the cellular CKAP4 level, the binding ability of spl3c to the BLCA 5637 cells decreased or increased, respectively (Fig. 2*E–H*). Moreover, the positive association between the spl3c binding ability and the CKAP4 expression in various cell types further confirmed the robustness of the spl3c–CKAP4 interaction (Fig. 2*I* and *J* and *SI Appendix*, Fig. S4). To elucidate the binding sites and interacting modes between spl3c and CKAP4, molecular docking was performed based on software Rosetta (Fig. 2*K* and *L* and *SI Appendix*, Fig. S8). Specifically, the binding between CKAP4 and spl3c was maintained by the formation of polar interactions, such as salt bridge and hydrogen bonds, as well as some hydrophobic contracts at the interface (*SI Appendix*, Table S1). Energy analysis also suggested the superior binding ability of truncated spl3c over spl3, the binding energy of which was reduced from -26.1 kcal/mol to -31.9 kcal/mol. To verify the direct interaction between CKAP4 and spl3c, an enzyme-linked oligonucleotide assay with whole-length CKAP4 (CKAP4_{WT}) and its extracellular-region depleted mutant (CKAP4_{Δ130–602}) was performed (*SI Appendix*, Fig. S9*B*); spl3c was able to bind to the CKAP4_{WT} at both 2 and 1 μg/mL, with a constant of 19.6 ± 2.8 and 30.9 ± 6.4 nM, respectively, similar to that in the BLCA 5637 cells (21.3 ± 6.6 nM, Fig. 1*H*). However, in the control group (CKAP4_{Δ130–602}), no evident binding of spl3c to CKAP4 was observed. Altogether, through an aptamer-based target discovery strategy, a molecular signature, CKAP4, was finally identified in BLCA cells.

High Expression of CKAP4 Is Associated with Malignancy of BLCA. To assess the significance of CKAP4 in BLCA malignancy, we first evaluated the CKAP4 gene alternation frequency, expression, and contribution to overall survival from open-access databases. Data showed that the gene alteration of CKAP4 in BLCA was relatively high, and amplification took up a major portion (Fig. 3*A*). The expression of CKAP4 was significantly higher in BLCA samples than in normal tissue samples (Fig. 3*B*). Moreover, the high level of CKAP4 in BLCA cells generally led to a worse overall survival (Fig. 3*C*). In pan-cancers, the elevated level of CKAP4 also showed worse overall survival and progression (*SI Appendix*, Fig. S10*A–C*).

To further verify the clinical significance of CKAP4 in BLCA, we evaluated the association between CKAP4 expression and the clinicopathologic characteristics of BLCA patients through immunohistochemical (IHC) analysis in a tissue microarray that included 176 BLCA and 16 noncancerous adjacent bladder tissues (*SI Appendix*, Table S2). As shown in Fig. 3*D–H*, CKAP4 expression was up-regulated in 165 out of 176 BLCA cases (positive rate = 93.75%) and was significantly associated with cancer stages and tumor–node–metastasis. Furthermore, as the gene sets analysis showed in Fig. 3*I* and *J* and *SI Appendix*, Fig. S10*D*, CKAP4 appeared to be highly associated with protein secretion and BLCA migration, which might imply the role of CKAP4 in BLCA metastasis. Collectively, these data indicate that up-regulated CKAP4 has a remarkable correlation with BLCA malignancy and

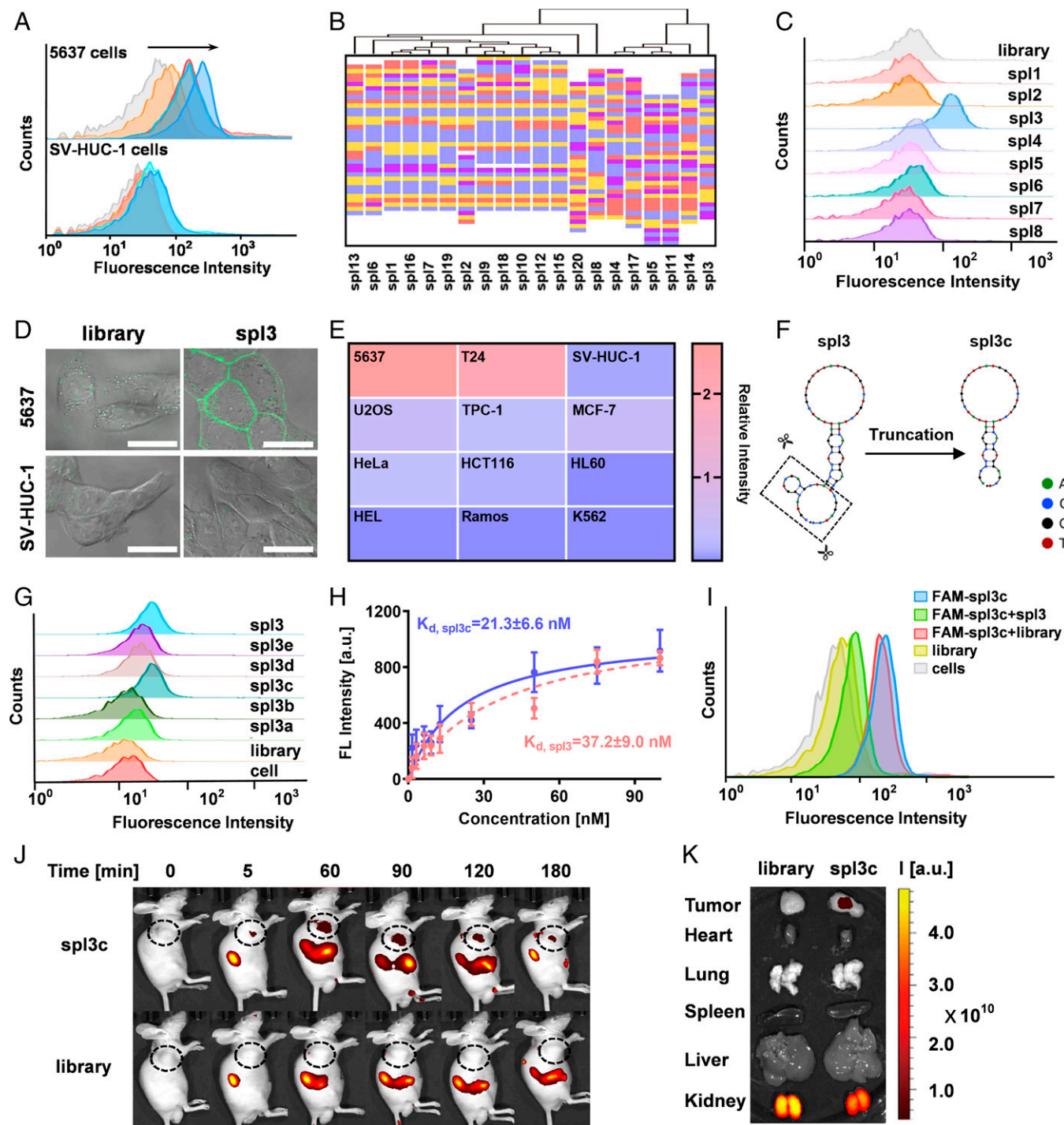


Fig. 1. Screening of an aptamer specifically targeting BLCA cells. (A) Flow cytometry to monitor the enrichment of the aptamer in the DNA pool. Binding of the DNA pool at the 5th, 8th, 11th, 13th, and 14th cycles are labeled as gray, orange, green, blue and red, respectively. (B) Hierarchy cluster analysis of the top 20 sequences in the 13th cycle DNA pool. A, T, C, and G are indicated as red, blue, pink, and yellow, respectively. (C) Flow cytometry results of aptamer candidates spl1-spl8 and library sequences to BLCA 5637 cells. (D) Binding specificity of spl3 to BLCA 5637 and SV-HUC-1 cells by confocal microscopy. (Scale bar: 20 μm.) (E) Binding ability of spl3 to an array of cell lines; row 1: urinary tract cell lines; rows 2 and 3: adherent cancer cell lines; row 4: leukemia cells. (F) Scheme of aptamer truncation. (G) Binding ability of truncated daughter aptamers of spl3 to BLCA 5637 cells by flow cytometry. (H) The dissociation constant (K_d) of spl3 (dashed line, red) and spl3c (solid line, blue) to BLCA 5637 cells. (I) Competition assay of spl3 and spl3c to BLCA 5637 cells. The concentration of spl3c was 250 nM, and those of spl3 and library were 2.5 μM. (J) In vivo binding of aptamer spl3c to BLCA 5637 cell-derived tumor. (K) Accumulation of aptamer spl3c in mouse organs.

that it may act as a potential biomarker in BLCA for progression and metastasis.

CKAP4 Orchestrates the Central-Peripheral Gradient of Stiffness on the Cell Surface. CKAP4 is one of the cytoskeleton-associated proteins and is highly relevant with cell membrane and organelles

such as the endoplasmic reticulum and the nucleus; however, how cell physical traits, such as cell stiffness, are regulated by CKAP4 remains unclear. To elucidate the effect of CKAP4 on cell mechanics, atomic force microscopy (AFM) was used to measure surface stiffness. As illustrated in Fig. 4A and B, when a force is applied on the cell, a soft surface is subjected to larger

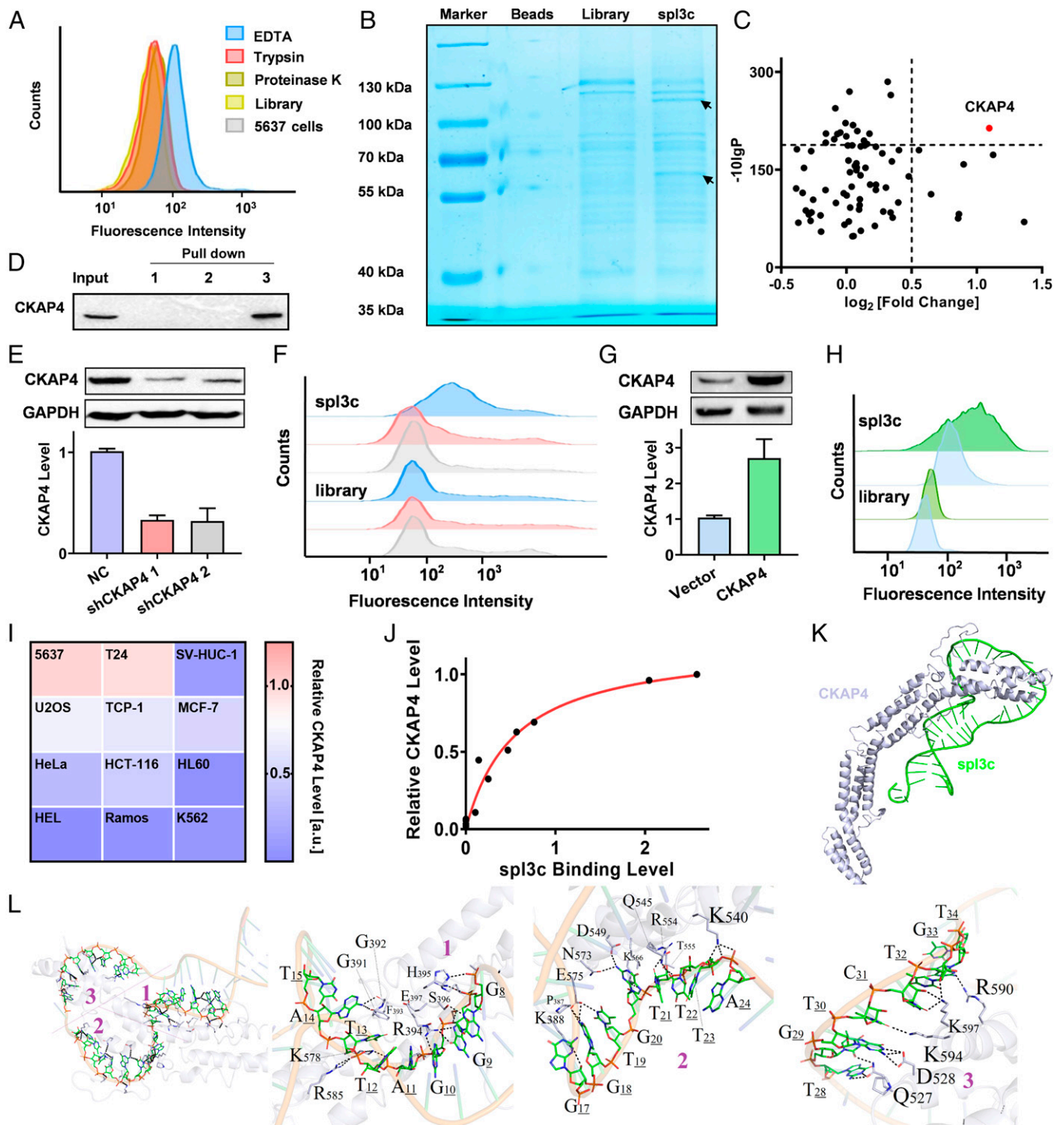


Fig. 2. Identification of aptamer spl3c-binding target on BLCA cells. (A) Identification of target type through cell membrane protein cleavage by trypsin and proteinase K. (B) Coomassie blue-stained SDS-PAGE was used to analyze aptamer-assisted target purification. The differential bands are indicated with black arrows. Beads refer to the naked beads, used as control. (C) Identification of the target of aptamer spl3c by MS score and fold change analysis. (D) Aptamer pull-down assay. Samples 1, 2, and 3 are the proteins pulled down by naked beads, DNA library-conjugated beads, and aptamer spl3c-conjugated beads, respectively. Samples were stained with a CKAP4 antibody. (E) Knockdown of CKAP4 in BLCA 5637 cells. (Upper) The CKAP4 level, as determined by Western blot, and (Lower) the corresponding quantification. NC, negative control; GAPDH, glyceraldehyde-3-phosphate dehydrogenase. (F) The binding of spl3c to CKAP4-depleted cells. NC, shCKAP4 1 and shCKAP4 2 were marked as blue, red and gray, respectively. (G) Overexpression of CKAP4 in 5637 cells. (Upper) The CKAP4 level, as determined by Western blot, and (Lower) the corresponding quantification. (H) Binding of spl3c to the CKAP4-up-regulated cells where vector and overexpression are marked as light blue and green, respectively. (I) CKAP4 expression level in various cell lines. Data were acquired by Western blot. (J) Correlation of spl3c binding level and CKAP4 level in various cancer cells. (K) Simulation of binding modes between spl3c and CKAP4. (L) Simulated binding sites between spl3c and CKAP4. Three representative binding sites were enlarged and are marked as 1, 2, and 3.

indentation, which leads to a steep slope in the force curve, while a stiff surface leads to less indentation with a relatively smooth slope. To clearly display the cell stiffness, a projection on the XY

plane is shown (Fig. 4C); the surface stiffness landscapes of the cells were highly associated with the level of CKAP4. When CKAP4 was highly expressed, the cell stiffness landscapes

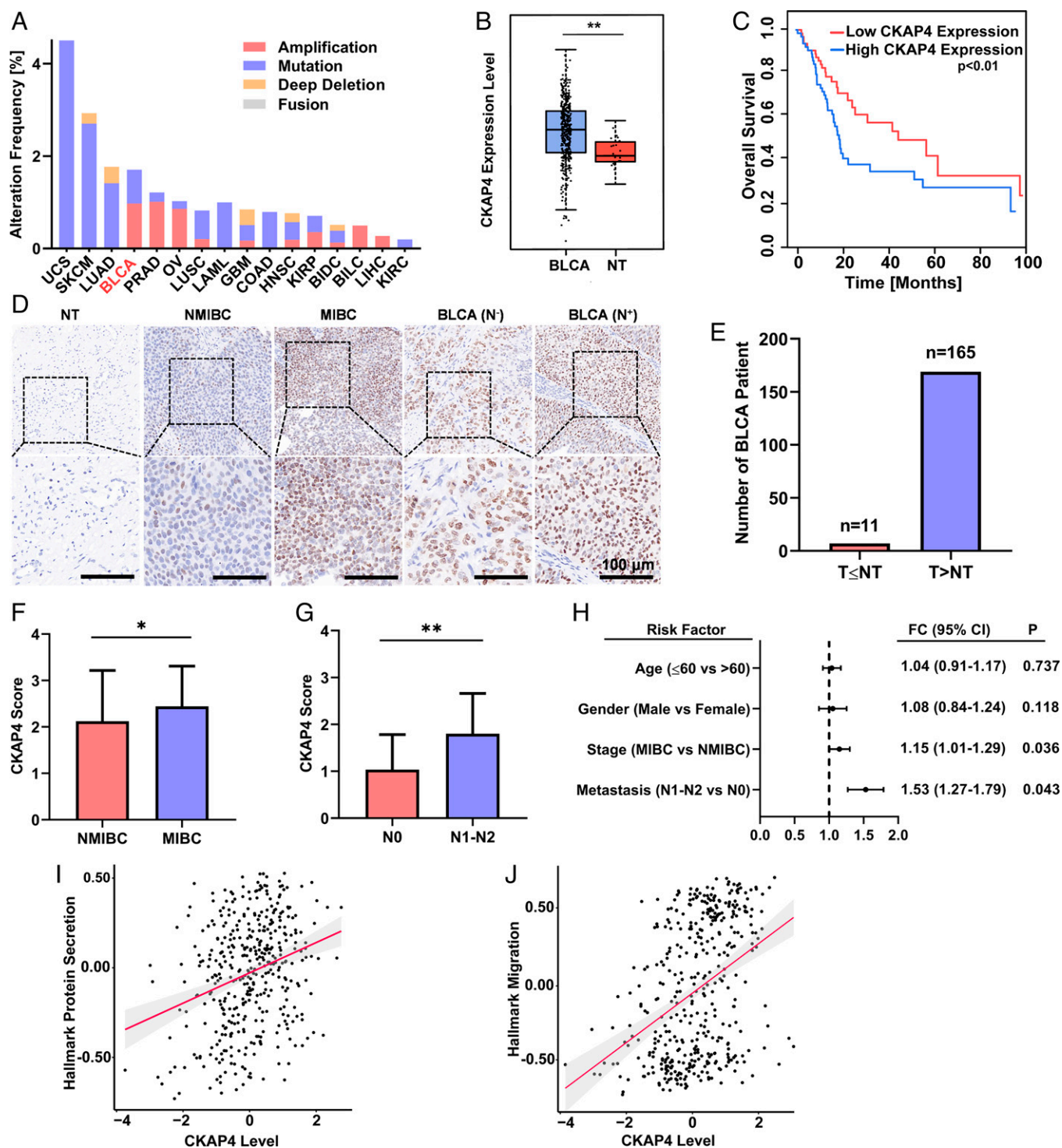


Fig. 3. The high expression of CKAP4 is associated with BLCA malignancy. (A) CKAP4 gene alteration frequency in pan-cancers from cBioPortal database. At least 200 cases were included in each type of cancer. UCS, uterine carcinosarcoma; SKCM, skin cutaneous melanoma; LUAD, lung adenocarcinoma; BLCA, bladder cancer; PRAD, prostate adenocarcinoma; OV, ovarian serous cystadenocarcinoma; LUSC, lung squamous cell carcinoma; LAML, acute myeloid Leukemia; GBM, glioblastoma multiforme; COAD, colon adenocarcinoma; HNSC, head and neck squamous cell carcinoma; KIRP, kidney renal papillary cell carcinoma; BILD, breast invasive lobular carcinoma; BILC, breast invasive ductal carcinoma; LIHC, liver hepatocellular carcinoma; KIRC, kidney renal clear cell carcinoma. (B) CKAP4 expression level in BLCA (404 cases) and NT (28 cases) from the Gepia2 database (mean \pm SEM, $**P < 0.01$, followed by unpaired Student's *t* test). NT, normal tissue. (C) Kaplan-Meier curve in BLCA patients with different levels of CKAP4 from the Tumor2.0 database, from which follow-up extended up to 100 mo with a split expression percentage of 15%. $P < 0.01$ was calculated by unpaired Student's *t* test. (D) Representative IHC staining images of CKAP4 level in NT and NMIBC, MIBC, T2 non-lymph-node metastasis (N⁻), and lymph node metastasis (N⁺) tissues. (Scale bar: 100 μ m.) MIBC, muscle invasive bladder cancer; NMIBC, nonmuscle invasive bladder cancer. (E) Number of CKAP4 up-regulated tumor samples compared with those of NT. If the score of the tumor tissue was higher than that of normal tissues, then it was defined as T $>$ NT; otherwise the score was defined as T \leq NT. NT, normal tissue; T, tumor tissue. (F) CKAP4 level in BLCA samples of NMIBC and MIBC (mean \pm SEM, $*P < 0.05$; unpaired Student's *t* test). (G) CKAP4 level in nonmetastatic (N0) and metastatic (N1-N2) BLCA in stage T2 (mean \pm SEM, $*P < 0.01$; unpaired Student's *t* test). (H) Forest plot shows the differential CKAP4 expression level. FC, fold change. (I) Association of CKAP4 level with hallmark protein secretion from GSEA database ($P = 8.6 \times 10^{-9}$; Pearson correlation test). (J) Association of CKAP4 level with hallmark migration from GSEA database ($P = 6.7 \times 10^{-16}$; Pearson correlation test).

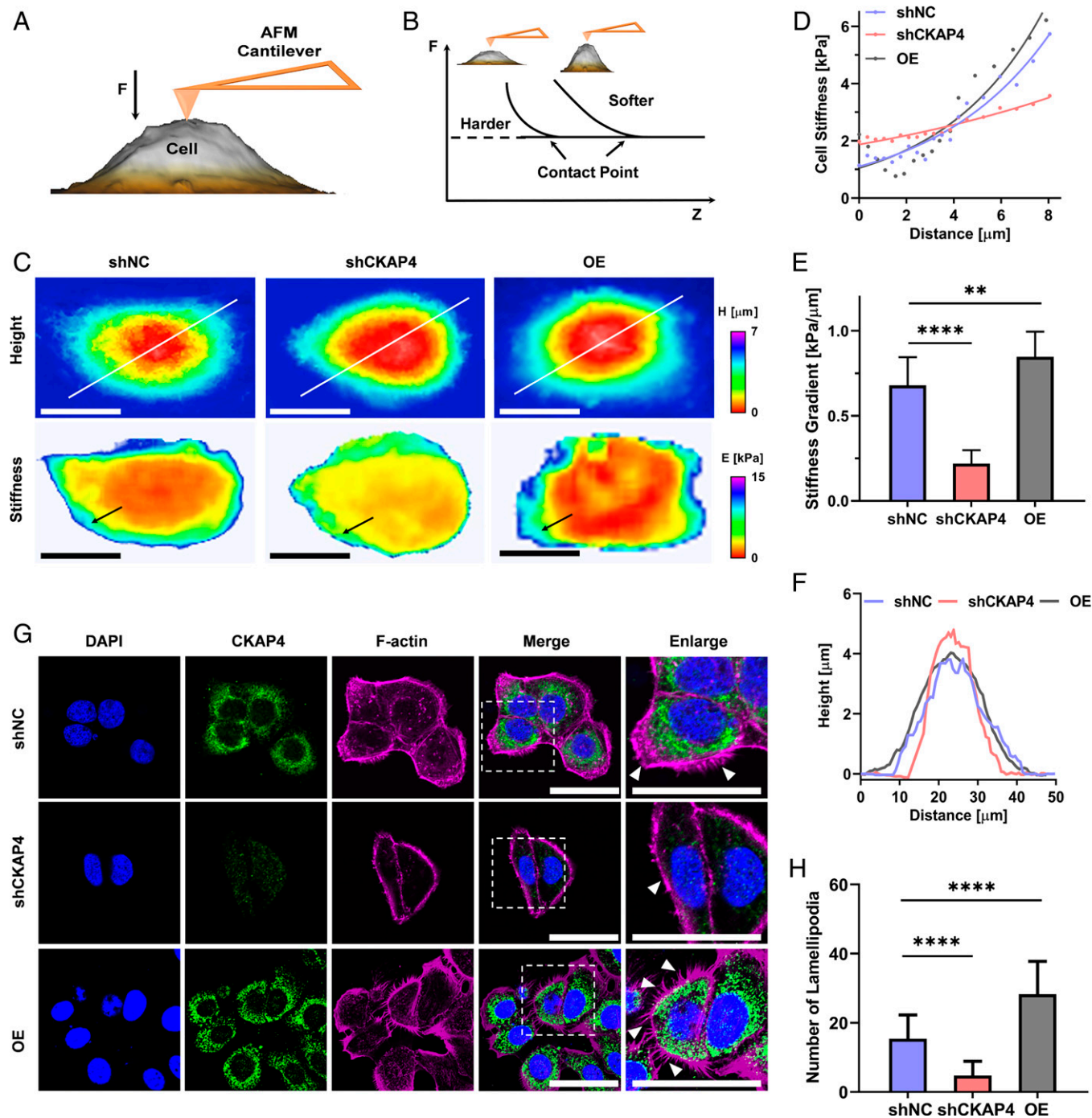


Fig. 4. CKAP4 orchestrates the central-peripheral gradient of cell stiffness. (A) Scheme represents the measurement of cell surface stiffness by AFM. (B) Force curves from AFM show the typical mechanical features of soft or stiff cell sample. (C) Height (Upper) and surface stiffness (Lower) of BLCA 5637 shNC, shCKAP4, and CKAP4 overexpressing (OE) cells. (Scale bar: 10 μm .) (D) Surface stiffness of BLCA 5637 shNC, shCKAP4, and CKAP4 OE cells across the indicated line in C. (E) Stiffness gradient of BLCA 5637 shNC, shCKAP4, and CKAP4 OE cells (mean \pm SEM, $n > 10$ cells, $**P < 0.01$; $****P < 0.0001$; unpaired Student's t test). (F) Surface height of BLCA 5637 shNC, shCKAP4, and CKAP4 OE cells across the indicated line in C. (G) CKAP4 expression level and F-actin in BLCA 5637 shNC, shCKAP4, and CKAP4 OE cells. CKAP4 was evaluated by antibody, and the nuclei were stained with Hoechst. (Scale bar: 20 μm .) (H) Quantification of lamellipodia of cells (mean \pm SEM, $n > 20$ cells, $****P < 0.0001$; unpaired Student's t test).

showed a central soft and peripheral stiff pattern; this physical trait was mitigated by CKAP4 depletion but enhanced by CKAP4 overexpression. As a result, a sharp stiffness gradient on the cell surface was sculpted: in the case of the BLCA 5637 shNC (short hairpin RNA for negative control) cells, the stiffness gradient across the cells was 0.68 ± 0.17 kPa/ μm , while in the CKAP4-depleted or CKAP4-overexpressed BLCA 5637 cells, the stiffness gradient across the cells was 0.22 ± 0.08

kPa/ μm or 0.85 ± 0.15 kPa/ μm , respectively (Fig. 4C–E). Similar gradients are also observed in projections on the XZ and YZ planes (SI Appendix, Fig. S11). To clarify the effects of substrate stiffness, the glass substrate was manipulated by coating it with a series of polyacrylamide gels. As seen in SI Appendix, Fig. S12, despite the substrate stiffness being remolded into different levels, the stiffness gradients of the cells were not altered significantly, further supporting the direct effect of CKAP4. In

addition, with a high expression of CKAP4, cells appeared to be a stretched phenotype with a relatively smooth curvature and the formation of lamellipodia (a typical phenotype for cell migration) (Fig. 4*F–H*). Such cells showed a wider spreading area and a more flattened morphology than CKAP4-depleted cells (*SI Appendix*, Fig. S13). Together, our observations in this part identified CKAP4 as a regulator of the architectural and mechanical features of cells.

CKAP4-Bearing Exosomes Intercellularly Transfer the Mechanical Traits of Cells. Exosomes are involved in the regulation of various cell behaviors, and the association of CKAP4 with secretion indicated in Fig. 3*I* suggested the possible existence of CKAP4 on exosomes (29). Whether the above-mentioned mechanical traits of cells can be transferred between BLCA cells via exosomes is an issue of interest and yet is largely unknown. In our study, we first isolated exosomes from BLCA 5637 (both shNC and shCKAP4 (short hairpin RNA for CKAP4)) and SV-HUC-1 cells and verified the expression of CKAP4 on exosomes (Fig. 5*A–C* and *SI Appendix*, Fig. S14) (30). Our data showed that CKAP4 was expressed in both BLCA 5637 cells and BLCA 5637-derived exosomes, and the depletion or low expression level of cellular CKAP4 led to a low level of exosomal CKAP4. Even in exosomes isolated from the urine of BLCA patients but not from that of healthy donors, CKAP4 showed high expression, further emphasizing the significance of exosomal CKAP4 in BLCA (*SI Appendix*, Fig. S15). The differential CKAP4 expression in exosomes showed no obvious influence on the physical properties of exosomes, such as size, shape, and surface charge, as well as their vesicle biology, such as secretion and uptake (*SI Appendix*, Fig. S16 and S17). When both the BLCA 5637 and SV-HUC-1 cells were cocultured with BLCA 5637 exosomes instead of up-regulated by exosomal contents, the exosomal CKAP4 could be effectively transported into these cells and allocated to both cytosol and the cell membrane (Fig. 5*D–G* and *SI Appendix*, Fig. S18 and S19). Consequently, the central stiffness of both 5637 and SV-HUC-1 cells significantly decreased and the peripheral stiffness underwent a slight increase, leading to an even sharper stiffness gradient on the cell surface (Fig. 5*H–L*). The effect of exosomal CKAP4 on cell stiffness was similar to what was observed in cells that underwent CKAP4 overexpression. Notably, the induced gradient of stiffness in the SV-HUC-1 cells was even sharper than that in the BLCA 5637 cells, potentially resulting from an even more marked increase of the cellular CKAP4 level through exosomal CKAP4 shuttling. These findings showed that CKAP4 served as a master mechanical regulator by orchestrating the surface stiffness gradient, and such mechanical traits could be transported through the intercellular shuttling of exosomal CKAP4.

CKAP4, as a Master Mechanical Regulator, Promotes Cell Migration, Which Is Enhanced by Exosome Shuttling. Having established CKAP4 as a regulator of central-peripheral gradient of cell stiffness, we next asked how such effects would influence cell behavior. First, we examined the effects on cell proliferation but observed no evident effects (*SI Appendix*, Fig. S20). Instead, cells exhibited active motility in the presence of CKAP4 (with a velocity of ~ 20 $\mu\text{m}/\text{h}$), whereas upon CKAP4 depletion, cell motility was significantly mitigated (only ~ 5 $\mu\text{m}/\text{h}$) to a level similar to that of noncancerous SV-HUC-1 cells, which was in line with the lamellipodia formation observed in Fig. 4*G*. Upon the internalization of CKAP4-harboring exosomes, the cell motility of all three cell types was increased, but such effects were not evident

upon the internalization of CKAP4-depleted exosomes (Fig. 6*A–C*). To further clarify the direct association between the stiffness gradient and cell migration, the stiffness gradient of cells was manipulated with a hypo- or hyperosmotic solution, and the cell migration was tracked accordingly. Consistently, the elevation of the stiffness gradient enhanced cell migration, and vice versa (*SI Appendix*, Fig. S21). Apart from single-cell migration, the presence of CKAP4 also influenced collective cell migration. As shown in Fig. 6*D*, the BLCA 5637 cells showed a rapid healing rate of the wound gap while upon CKAP4 depletion, the healing rate was mitigated significantly. After the internalization of CKAP4-bearing exosomes but not CKAP4-depleted exosomes, the migration rate was boosted (Fig. 6*E*). Moreover, the transmigration ability of the BLCA 5637 cells was significantly higher than that of the CKAP4-depleted cells, and after the internalization of CKAP4-bearing but not CKAP4-depleted exosomes, the transmigration ability of cells was enhanced in both the shNC and shCKAP4 groups (Fig. 6*F* and *G*). The effect of CKAP4 in promoting cell migration was also supported by the formation of lamellipodia and the enhanced cell adhesion (Fig. 4*G* and *SI Appendix*, Fig. S22 and S23).

Metastasis of BLCA Cells Is Promoted by Cellular and Exosomal CKAP4. To investigate the potential of CKAP4 in driving BLCA metastasis, we established a tail vein injection metastasis model. As illustrated in Fig. 7*A*, 5×10^6 BLCA 5637 shNC and shCKAP4 cells were respectively injected into mice from the tail vein. Eight weeks later, mice were killed and dissected for metastatic analysis. With hematoxylin and eosin (H&E), Ki-67, and CKAP4 staining, marked tumor nodules were visible in both the liver and lung of mice in the shNC group (panel i), while upon CKAP4 depletion, almost no metastatic nodules were shown (panel ii) (Fig. 7*C* and *SI Appendix*, Fig. S24*A*). To further uncover the role of exosomal CKAP4 in BLCA metastasis, cells were first pretreated with exosomes for 12 h, injected in mice from the tail vein, and then further treated with exosomes every 2 wk from the fourth week (Fig. 7*A*). The detailed information about cell and exosome treatment in the different groups is shown in Fig. 7*B*. Our data demonstrated that CKAP4-bearing exosomes significantly enhanced the metastasis of BLCA cells in both shNC and shCKAP4 groups (panel iii–iv), while CKAP4-depleted exosomes showed no such effects (panel v–vi) (Fig. 7*C–F* and *SI Appendix*, Fig. S24*A–D*). As shown in Fig. 7*D* and *SI Appendix*, Fig. S24*B*, the metastatic potential of BLCA cells was increased approximately twofold upon the treatment with CKAP4-harboring exosomes, while CKAP4-depleted exosomes showed almost no effect on BLCA metastasis. Considering the long duration in the metastasis of BLCA cells, the maintenance of phenotypes after exosome treatment was tracked over time (*SI Appendix*, Fig. S25). Our results showed that cell division played a major role in exosomal CKAP4-induced cancerous phenotype changes; therefore, in metastatic events, exosomal CKAP4 would exert durable effects until cell division after settlement in organs. Taken together, our results offered *in vivo* insight into cellular and exosomal CKAP4 as drivers of BLCA metastasis.

Discussion

In this work, we develop an aptamer-based molecular tool, spl3c, that can recognize its target CKAP4 protein overexpressed on BLCA cells. The robust interaction of spl3c and CKAP4 highlights the promising potential of aptamer-based biomarker discovery. Considering its specificity to BLCA cells and BLCA-derived

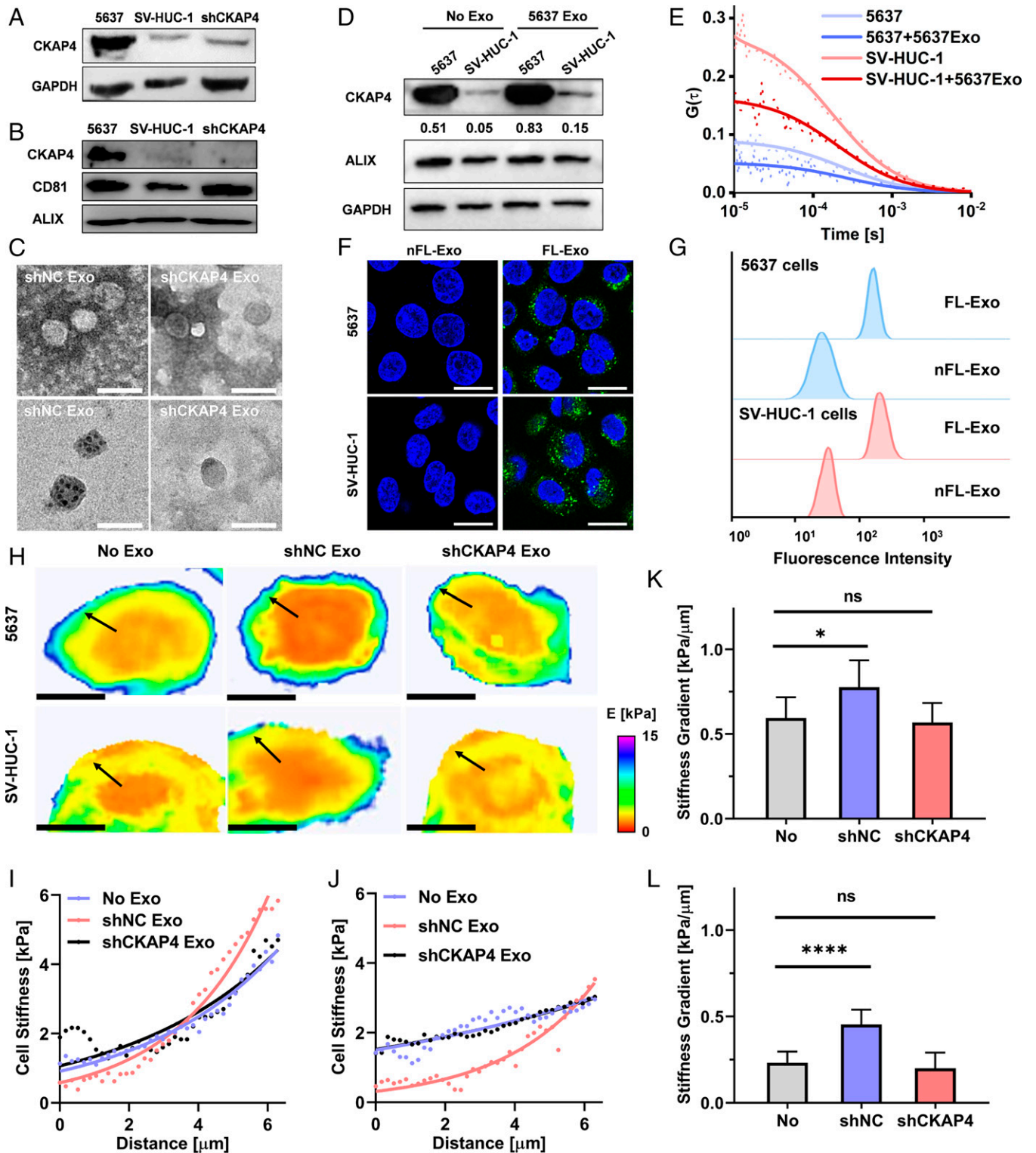


Fig. 5. Exosomal CKAP4 enhances the central-peripheral gradient of cell stiffness. (A) CKAP4 level in BLCA 5637 shNC, SV-HUC-1 cells, and shCKAP4. (B) CKAP4 level in BLCA 5637 shNC-, SV-HUC-1-, and shCKAP4-derived exosomes. CD81 and ALIX were used as biomarkers of the exosomes. (C) Transmission electron microscopy (TEM) images of exosomes isolated from BLCA 5637 shNC and shCKAP4 cells (*Upper*); labeling of BLCA 5637 shNC and shCKAP4 exosomes with spl3c-conjugated 5 nM gold nanoparticles (*Lower*). (Scale bar: 100 nm.) (D) CKAP4 level of cells treated with or without BLCA 5637 shNC exosomes by Western blot. (E) Surface CKAP4 level of BLCA 5637 and SV-HUC-1 cells treated with or without BLCA 5637 shNC exosomes is identified with FITC-labeled spl3c using fluorescence correlation spectroscopy. (F) Fluorescence level of BLCA 5637 and SV-HUC-1 cells after treatment with 5637 exosomes (nFL-Exo) or GFP-CKAP4-expressing 5637 exosomes (FL-Exo) using confocal microscopy. (Scale bar: 20 μm .) GFP, green fluorescent protein. (G) Fluorescence level of 5637 and SV-HUC-1 cells after treated with nFL-Exo or FL-Exo by flow cytometry. (H) Surface stiffness of BLCA 5637 cells (*Upper*) and SV-HUC-1 cells (*Lower*) treated with or without exosomes. Representative images are shown. (Scale bar: 10 μm .) (I and J) Surface stiffness of BLCA 5637 (I) and SV-HUC-1 (J) cells across the indicated line in H. (K and L) Stiffness gradient of BLCA 5637 (K) and SV-HUC-1 (L) cells (mean \pm SEM; $n > 10$ cells; ns, not significant; $*P < 0.05$; $****P < 0.0001$; unpaired Student's *t* test).

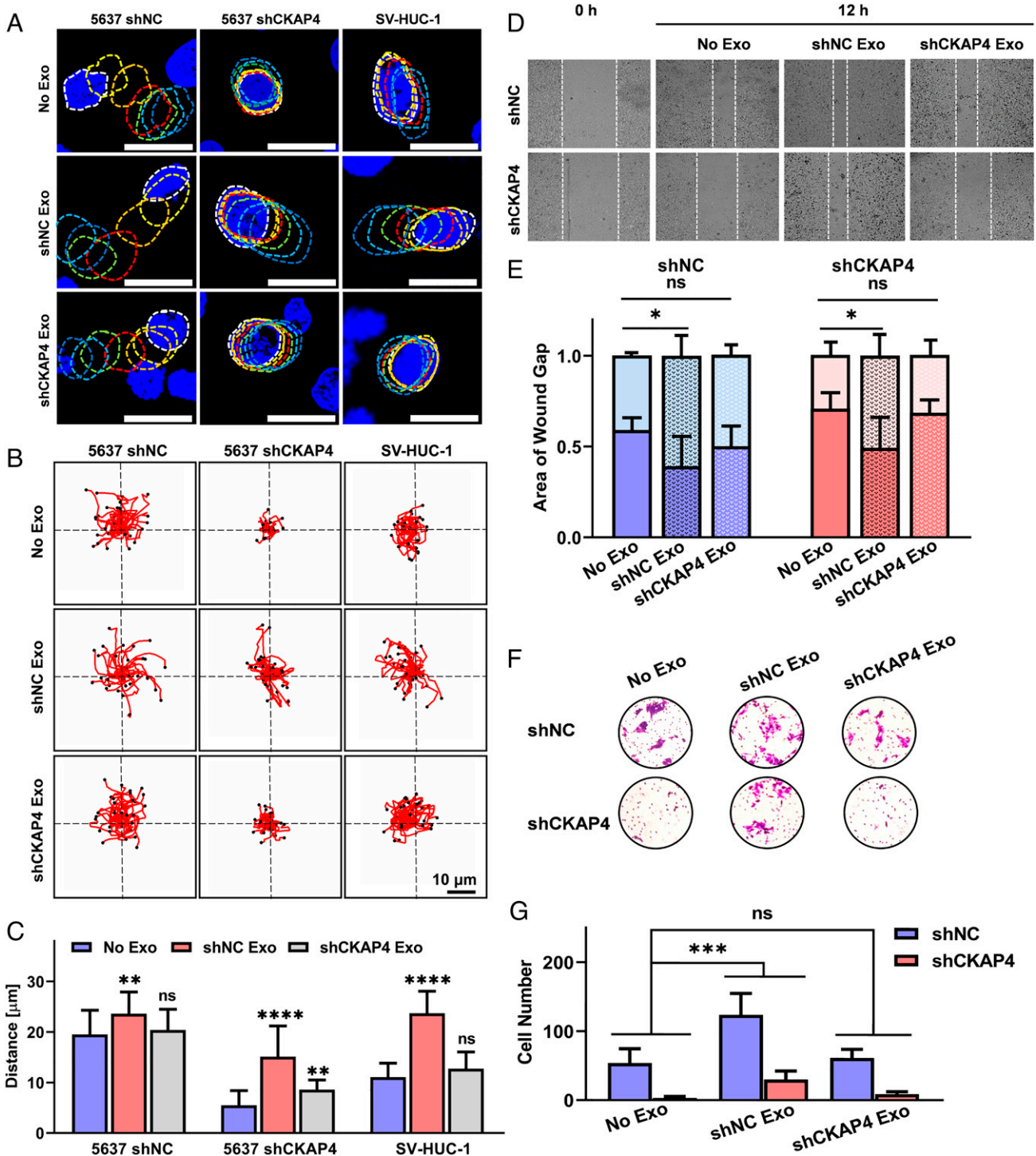


Fig. 6. Cell motility and cell migration are promoted by cellular and exosomal CKAP4. (A) Single-cell motility of 5637 NC, 5637 shCKAP4 cells, and SV-HUC-1 cells, as well as the influence of the CKAP4-harboring and CKAP4-depleted 5637 exosomes. Each circle-shaped contour represents the movement of a cell in 10 min. (Scale bar: 20 μ m.) (B) Trajectory trace analysis of 5637 NC, 5637 shCKAP4 cells, and SV-HUC-1 cells, as well as the influence of CKAP4-harboring and CKAP4-depleted 5637 exosomes. (C) Motility of cells measured in the time scale of 1 h (mean \pm SEM; $n > 30$ cells; ns, not significant; $**P < 0.01$, $****P < 0.0001$; unpaired Student's t test). (D and E) Wound healing assay of 5637 NC and shCKAP4 cells, as well as the effect of CKAP4-bearing and CKAP4-depleted 5637 exosomes (mean \pm SEM, $n = 3$ independent experiments, $*P < 0.05$; unpaired Student's t test). (F and G) Trans-well assay of 5637 NC and shCKAP4 cells, as well as the effect of CKAP4-bearing and CKAP4-depleted 5637 exosomes (mean \pm SEM, $n = 3$ independent experiments, $***P < 0.001$; unpaired Student's t test).

exosomes, spl3c has the potential to be developed for noninvasive BLCA diagnostics and therapies in clinics.

CKAP4 is known as a plasma membrane receptor and intracellular regulator in both normal cells and cancer cells (31–34), yet its role in cell mechanics is rarely investigated. In this work, our results demonstrate the effect of CKAP4 in maintaining a

favorable mechanical phenotype—that is, a sharp stiffness gradient on the cell surface—thereby promoting the motility, migration, and metastasis of BLCA cells. Importantly, our work adds more in-depth insights on the paradox that either stiffening or softening aggravates cancer malignancy (24, 35, 36): instead of regional stiffening or softening of the cell, the CKAP4-induced surface stiffness

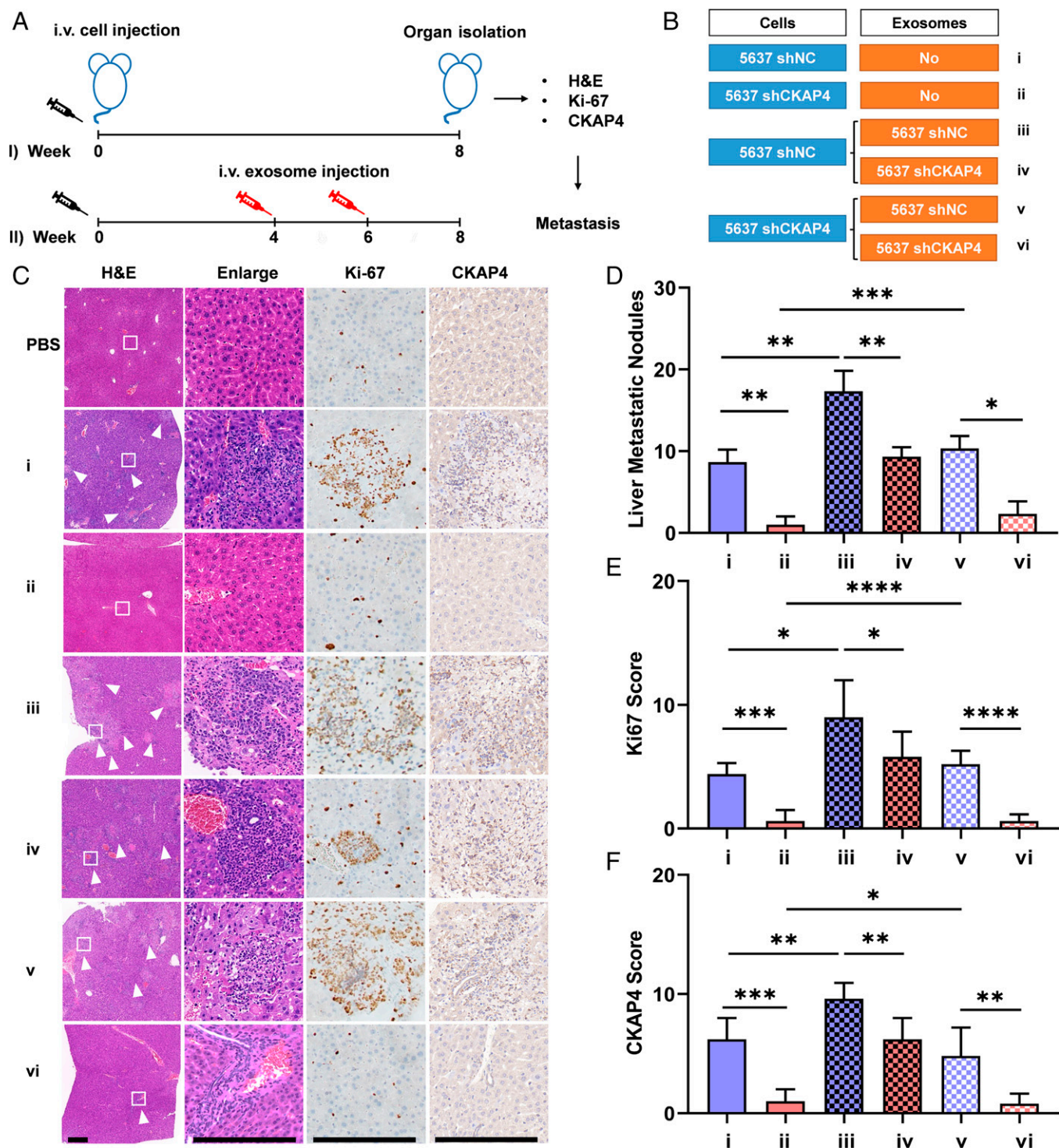


Fig. 7. CKAP4 promotes the metastasis of BLCA cells. (A) Time schedule of intravenous injection of cells (I) and exosomal pretreated cells (II) into mice and subsequent analysis at 8 wk postinjection. (B) Cellular data for intravenous injection in mice. Groups i and ii were not treated with exosomes; groups iii–vi were pretreated with 5637 shNC or shCKAP4 exosomes. (C) The liver metastasis of cells in B was determined by H&E, Ki-67, and CKAP4 staining. Representative images of three independent experiments are shown. (Scale bar: 1 mm.) (D) The average number of liver metastatic nodules. (E) The Ki-67 score of liver metastatic nodules. (F) The CKAP4 score of liver metastatic nodules (mean \pm SEM, $n = 3$ independent experiments, $*P < 0.05$; $**P < 0.01$; $***P < 0.001$; $****P < 0.0001$; unpaired Student's t test). (D–F) blue and red bars represent BLCA 5637 shNC and shCKAP4 cells, respectively; black grids refer to BLCA 5637 cells pre-treated with BLCA 5637 shNC and shCKAP4 exosomes, respectively; and white grids refer to BLCA 5637 shCKAP4 cells pretreated with BLCA 5637 shNC and shCKAP4 exosomes, respectively.

gradient plays a more dominant role in cancer metastasis. Interestingly, due to the expression of CKAP4 on exosomes, the mechanical traits can also be intercellularly transported through exosomal CKAP4 shuttling; therefore, our study identifies an exosome-based pathway of the transportation of cell mechanics.

In conclusion, our work suggests the advantages of the aptamer-based target discovery strategy in a molecular-profile exploration of cancer cells, highlights the significance of the central-peripheral gradient of stiffness in cancer malignancy, and validates a pathway of the transportation of cell mechanical traits.

Materials and Methods

A more detailed description of all materials and methods is given in the *SI Appendix*.

Cell-SELEX Procedures. The Cell-SELEX process against BLCA 5637 cells and normal bladder epithelial SV-HUC-1 cells was performed as previously reported (27, 28), based on confocal microscopy and flow cytometry (details in *SI Appendix, Methods*).

Identification of Aptamer Target. The aptamer target from cell lysates was pulled down by spl3c-conjugated beads and identified by MS (details in *SI Appendix, Methods*).

Cellular Young's Modulus Measurement. The force spectra were mapped with a DNP-10 probe (0.06 N/m) using a JPK Nanowizard 4 atomic force spectroscopy, the spring constant and sensitivity of the cantilever were calibrated by thermal noise signals in contact mode, and cells were observed with an Olympus confocal microscope in bright-field. A Hertz model was chosen for the fitting of the force curve using JPKSPM data processing software (details in *SI Appendix, Methods*).

IHC. IHC was performed on formaldehyde-fixed and paraffin-embedded tissue sections, which were stained with H&E, Ki-67, and CKAP4 antibody. Images were taken with a DIM6000 (Leica) microscope. Images were analyzed with Image J and CaseViewer software (details in *SI Appendix, Methods*).

1. C. H. Stuelten, C. A. Parent, D. J. Montell, Cell motility in cancer invasion and metastasis: Insights from simple model organisms. *Nat. Rev. Cancer* **18**, 296–312 (2018).
2. H. Dillekäs, M. S. Rogers, O. Straume, Are 90% of deaths from cancer caused by metastases? *Cancer Med.* **8**, 5574–5576 (2019).
3. D. A. Fletcher, R. D. Mullins, Cell mechanics and the cytoskeleton. *Nature* **463**, 485–492 (2010).
4. S. van Helvert, C. Storm, P. Friedl, Mechanoreciprocity in cell migration. *Nat. Cell Biol.* **20**, 8–20 (2018).
5. S. Massouf *et al.*, Cell stretching is amplified by active actin remodelling to deform and recruit proteins in mechanosensitive structures. *Nat. Cell Biol.* **22**, 1011–1023 (2020).
6. D. L. Bodor, W. Pönisch, R. G. Endres, E. K. Paluch, Of cell shapes and motion: The physical basis of animal cell migration. *Dev. Cell* **52**, 550–562 (2020).
7. P. H. Wu *et al.*, Single-cell morphology encodes metastatic potential. *Sci. Adv.* **6**, eaaw6938 (2020).
8. E. L. Batchelder *et al.*, Membrane tension regulates motility by controlling lamellipodium organization. *Proc. Natl. Acad. Sci. U.S.A.* **108**, 11429–11434 (2011).
9. Z. Razinia *et al.*, Stiffness-dependent motility and proliferation uncoupled by deletion of CD44. *Sci. Rep.* **7**, 16499 (2017).
10. J. Rheinlaender *et al.*, Cortical cell stiffness is independent of substrate mechanics. *Nat. Mater.* **19**, 1019–1025 (2020).
11. H. T. Nia, L. L. Munn, R. K. Jain, Physical traits of cancer. *Science* **370**, 1–11 (2020).
12. V. Panzetta *et al.*, Mechanical phenotyping of cells and extracellular matrix as grade and stage markers of lung tumor tissues. *Acta Biomater.* **57**, 334–341 (2017).
13. D. A. Rudzka *et al.*, Migration through physical constraints is enabled by MAPK-induced cell softening via actin cytoskeleton re-organization. *J. Cell Sci.* **132**, jcs224071 (2019).
14. J. M. Jaslove, C. M. Nelson, Smooth muscle: A stiff sculptor of epithelial shapes. *Philos. Trans. R. Soc. Lond. B Biol. Sci.* **373**, 1–12 (2018).
15. P. Sens, J. Plastino, Membrane tension and cytoskeleton organization in cell motility. *J. Phys. Condens. Matter* **27**, 273103 (2015).
16. A. R. Houk *et al.*, Membrane tension maintains cell polarity by confining signals to the leading edge during neutrophil migration. *Cell* **148**, 175–188 (2012).
17. A. S. Kashani, M. Packirisamy, Cancer cells optimize elasticity for efficient migration. *R. Soc. Open Sci.* **7**, 200747 (2020).
18. A. Diz-Muñoz, D. A. Fletcher, O. D. Weiner, Use the force: Membrane tension as an organizer of cell shape and motility. *Trends Cell Biol.* **23**, 47–53 (2013).
19. A. Schaefer *et al.*, Actin-binding proteins differentially regulate endothelial cell stiffness, ICAM-1 function and neutrophil transmigration. *J. Cell Sci.* **127**, 4470–4482 (2014).

Data Availability. All study data are included in the article and/or *SI Appendix*.

ACKNOWLEDGMENTS. This work was supported by grants from the National Key Research and Development Program of China (2021YFA0909403), the National Natural Science Foundation of China (21890744, 81672760, 91959102, 82003286, and 61527806), the Changsha Science and Technology Project (kq2001012), the fellowship of the China Postdoctoral Science Foundation (2020M672474, 2020M682539), the Science and Technology Innovation Program of Hunan Province (2020RC2021), and the Changsha Municipal Natural Science Foundation (kq2014041).

Author affiliations: ^aMolecular Science and Biomedicine Laboratory, State Key Laboratory of Chemo/Biosensing and Chemometrics, College of Biology, College of Chemistry and Chemical Engineering, Aptamer Engineering Center of Hunan Province, Hunan University, Changsha, Hunan 410082, China; ^bThe Cancer Hospital of the University of Chinese Academy of Sciences (Zhejiang Cancer Hospital), Institute of Basic Medicine and Cancer, Chinese Academy of Sciences, Hangzhou, Zhejiang 310022, China; ^cMolecular Biology Research Center, Central South University, Changsha, Hunan 410078, China; ^dCenter for Medical Genetics, School of Life Sciences, Central South University, Changsha, Hunan 410078, China; ^eCenter of Orbital and Oculoplastic Surgery, The Eye Hospital of Wenzhou Medical University, Wenzhou, Zhejiang 325027, China; and ^fDepartment of Urology, 2nd XiangYa Hospital, Central South University, Changsha, Hunan 410078, China

Author contributions: X.S., H.L., M.Y., and W.T. designed research; X.S., L.X., S.Q., H.L., Y. Zhou, H.Z., Y. Zhang, Lin Zhang, T.X., Y.C., and Lili Zhang performed research; Lei Zhang contributed new reagents/analytic tools; X.S., S.Q., Z.Z., T.P., J. Liu, W.W., J. Li, M.Y., and W.T. analyzed data; and X.S., J. Li, M.Y., and W.T. wrote the paper.

20. J. M. Kalapurakkal *et al.*, Integrin mechano-chemical signaling generates plasma membrane nanodomains that promote cell spreading. *Cell* **177**, 1738–1756.e23 (2019).
21. A. Bisaria, A. Hayer, D. Garbett, D. Cohen, T. Meyer, Membrane-proximal F-actin restricts local membrane protrusions and directs cell migration. *Science* **368**, 1205–1210 (2020).
22. B. Cheng *et al.*, Nanoscale integrin cluster dynamics controls cellular mechanosensing via FAKY397 phosphorylation. *Sci. Adv.* **6**, eaax1909 (2020).
23. K. Keren *et al.*, Mechanism of shape determination in motile cells. *Nature* **453**, 475–480 (2008).
24. F. Zancanato, M. Cordenonsi, S. Piccolo, YAP/TAZ at the roots of cancer. *Cancer Cell* **29**, 783–803 (2016).
25. T. Panciera, L. Azzolin, M. Cordenonsi, S. Piccolo, Mechanobiology of YAP and TAZ in physiology and disease. *Nat. Rev. Mol. Cell Biol.* **18**, 758–770 (2017).
26. S. S. Ranade *et al.*, Piezo1, a mechanically activated ion channel, is required for vascular development in mice. *Proc. Natl. Acad. Sci. U.S.A.* **111**, 10347–10352 (2014).
27. X. Wu *et al.*, Elucidation and structural modeling of CD71 as a molecular target for cell-specific aptamer binding. *J. Am. Chem. Soc.* **141**, 10760–10769 (2019).
28. H. Li *et al.*, A novel aptamer LL4A specifically targets vemurafenib-resistant melanoma through binding to the CD63 protein. *Mol. Ther. Nucleic Acids* **18**, 727–738 (2019).
29. G. Rodrigues *et al.*, Tumour exosomal CEMIP protein promotes cancer cell colonization in brain metastasis. *Nat. Cell Biol.* **21**, 1403–1412 (2019).
30. G. Corso *et al.*, Systematic characterization of extracellular vesicle sorting domains and quantification at the single molecule-single vesicle level by fluorescence correlation spectroscopy and single particle imaging. *J. Extracell. Vesicles* **8**, 1663043 (2019).
31. P. A. Sandoz, F. G. van der Goot, How many lives does CLIMP-63 have? *Biochem. Soc. Trans.* **43**, 222–228 (2015).
32. L. Gao *et al.*, The RBP1-CKAP4 axis activates oncogenic autophagy and promotes cancer progression in oral squamous cell carcinoma. *Cell Death Dis.* **11**, 488–503 (2020).
33. Y. Osugi, K. Fumoto, A. Kikuchi, CKAP4 regulates cell migration via the interaction with and recycling of integrin. *Mol. Cell Biol.* **39**, 1–18 (2019).
34. Q. Lyu *et al.*, SENCER stabilizes vascular endothelial cell adherens junctions through interaction with CKAP4. *Proc. Natl. Acad. Sci. U.S.A.* **116**, 546–555 (2019).
35. K. Keren, T. Shemesh, Buckle up: Membrane tension drives lamellipodial network compression and adhesion deposition. *J. Cell Biol.* **216**, 2619–2621 (2017).
36. D. Raucher, M. P. Sheetz, Cell spreading and lamellipodial extension rate is regulated by membrane tension. *J. Cell Biol.* **148**, 127–136 (2000).